Control and Cybernetics

vol. **47** (2018) No. 4

Response surface methodology assisted multi-objective optimization of TIG process for 15CDV6 steel

by

P. D. Skariya[1], M. Satheesh[1], J. Edwin Raja Dhas[1] and G. Chandrasekar[2]

[1]Noorul Islam Centre for Higher Education, Thuckalay, Tamil Nadu, India - 629180
skariyapd2005@gmail.com
[2]PSNA College of Engineering & Technology, Dindigul, Tamilnadu, India - 624622

Abstract: Welding is a way of heating pieces of metal using electricity or flame so that they melt and stick together. There are many kinds of welding processes, such as, for instance, MIG/MAG and MMA welding. However, such welding schemes require more electrodes during the process of welding. Hence, this paper intends to analyse the alternative tungsten inert gas (TIG) welding technology using Response Surface Methodology (RSM), and to identify the effect of TIG welding process parameters on the weld bead profile of 15CDV6 high strength low alloy (HSLA) steel. Moreover, the methodology applied allows for identification of the optimal welding conditions by means of multi-objective optimization using RSM to increase the depth of penetration (DOP) and reduce BW (bead width) and heat-affected zone (HAZ) width. The variables taken for the model-based investigations are: welding current (W_c), torch speed (T_s), gas flow rate (G_r), torch angle (T_a) and arc gap (A_g). Moreover, the responses taken are DOP, BW and HAZ width. Further, the results from the proposed model optimisation can be seen as highly beneficial for the rocket-motor hardware program, industries and fabrication of pressure vessels, which are using 15CDV6 steel.

Keywords: TIG welding, 15CDV6 HSLA steel, depth of penetration, bead width, HAZ width

1. Introduction

HSLA steels have been initially introduced to substitute low carbon steels for the aerospace and automotive industry with the intention to enhance the strength-to-weight ratio, together with improved weldability and formability. HSLA steel offers distinctive features like ductability, better yield strength, and temperature control, as well as toughness. HSLA steel features strength in the range

Table 1. Notations used throughout the paper

Abbreviation	**Meaning**
AES	Atomic emission spectroscopy
AR	Aspect ratio
ATIG	Activated TIG
BH	Bead height
BM	Base metal
BR	Brightness ratio
BW	Bead width
CCD	Central composite design
DCEN	Direct current electrode negative
DOE	Design of experiments
DOP	Depth of penetration
DP	Depth of penetration
EDM	Electrical discharge machining
GA	Genetic algorithm
GTAW	Gas tungsten arc welding
HAZ	Heat-affected zone
HI	Heat input
HSLA	High strength low alloy
KM	Kriging model
LSP	Laser shock penning
MIG	Metal inert gas
MAG	Metal active gas
MMA	Manual metal arc welding
OPP	Optimum process parameters
Ra	Surface roughness
RAFM	Reduced activation ferritic/martensitic
RSM	Response surface methodology
SEM	Scanning electron microscope
SG	Shielding gas
TIG	Tungsten inert gas
UP-ATIG	Un-peened ATIG
W_c	Welding current
T_s	Torch speed
G_r	Gas flow rate,
T_a	Torch angle
A_g	Arc gap
D	Molybdenum
Cr	Chromium
V	Vanadium

of 250-590 megapascals. Moreover, its improved strength and its other characteristics are of high value for building constructions, pressure vessels, rocket motor casings, and shipping (Tracy, Nelson and Rose, 2016). The 15CDV6 is low carbon high strength bainitic steel, which belongs to HSLA group, which includes low concentrations of D, Cr, and V as alloying components (see the table below). It is a Cr-Mo-V steel with excellent weldability. In addition, welding of 15CDV6 can be performed without pre-heating up to the thickness of 10 mm and joint processing strength of 1000 Mpa can be attained in the absence of heat treatments (see Thompson, 2018; Luo et al., 2018).

Weight %	Alloy 15CDV6
C	0.12-0.18
P	Max 0.020
Si	Max 0.20
V	0.20-0.30
Mn	0.08-1.1
S	Max 0.015
Cr	0.25-1.5
Mo	0.80-1.00
Fe	balance

15CDV6 composition specifications, after, e.g.
https://www.aircraftmaterials.com/data/alstst/15cdv6.html

A well-known welding process, exploited for merging the RAFM steels, is the so-called TIG welding (Chellappan, Lingadurai and Sathiya, 2017). TIG welding is selected for arc welding procedure, owing to its high quality weld deposits. The TIG welding process (Singh, Dey and Rai, 2017; Chen et al., 2017a) is the most important welding method presently exploited in the thermal and nuclear power plant industries for manufacturing of the different constituents, primarily in view of its capability to generate high-quality welds (Chen et al., 2017b; Wang et al., 2018). On the other hand, though, limitations, related to the uncontrolled weld penetration, owing to negligible differentiation in alloying elements, or low single pass penetration, and the necessity of applying numerous passes for thick gauge sections cause that it is regarded as less productive (Piekarska and Rek, 2017; Junaid et al., 2017).

Duplex stainless steel components are usually formed by means of arc welding processes (Ai et al., 2016; Shi, Zheng and Huang, 2013; Yang et al., 2013). TIG welding (Prasad et al., 2016; Costa et al., 2016) is favored over other arc welding processes owing to its high-quality weld deposit. The major advantage of the TIG welding procedure consists in improved mechanical and metallurgical properties, and the restriction is the lower DOP during autogenous welding, resulting in lower productivity (Longlong et al., 2016; Yan et al., 2017; Chinchole, 2016). The most important drawback of TIG welding procedure is its relatively

shallow penetration capacity in single pass welding (Liang et al., 2017; Meng et al., 2014). The shallow depth of penetration (DOP) may result in the failure of a welded structure (Srirangan and Paulraj, 2016; Hirose et al., 2015), since penetration determines the stress carrying capacity of a welded joint (Zou et al., 2015; Nagesh and Datta, 2010). The welding process input parameters, which influence the bead geometry, must, therefore, be properly selected in order to obtain a high quality joint (Chen et al., 2014).

This paper contributes to the development of the TIG welding by proposing improved welding characteristics using RSM, and also analyzes the effect of TIG welding process parameters on the characteristics of 15CDV6 HSLA steel. In addition, we identify the desired conditions for optimal welding by employing multi-objective optimization to increase the DOP and minimize the HAZ and BW. The paper is organized as follows. Section 2 discusses the related work and reviews the results obtained to date. Section 3 describes the design of the experiment and Section 4 presents the modeling of the TIG welding through regression analysis. Section 5 analyses the optimization of welding parameters and Section 6 shows the validation tests. Section 7 is devoted to the practical implications, while Section 8 sums up the paper.

2. Literature review

2.1. Related works

In 2014, Korra, Vasudevan and Balasubramanian (2014) suggested a new scheme, in which the input process parameters were varied at 5 levels, which resulted in 21 trail experiments. Bead-onplate welds were carried out on 10-mm-thick duplex stainless steel plates. The characteristics such as BW, DOP, BH, area of DOP, AR, and HAZ width were calculated following the experiments. Moreover, a second-order response surface design was introduced for response prediction for the group of specified input factors. Subsequently, multi-objective optimization was carried out to acquire the required weld bead geometry by means of the desirability scheme.

Then, Vasantharaja and Vasudevan (2015) suggested a scheme, in which the major issue in choosing the optimum input parameters was resolved by applying the RSM. The central composite model of RSM was exploited in order to produce the design matrix for producing data on the manipulation of ATIG (activated TIG) welding process parameters. In addition, the input variables, such as torch speed, welding current, arc gap and electrode tip angle were taken into consideration for assessment. A second-order response surface design was established for developing the response for a group of known input factors. Subsequently, mathematical and graphical optimization was carried out by means of RSM to obtain the required BW, DOP and target HAZ width.

Yet later, Srivastava and Garg (2017) introduced a scheme, which analyses the effect of a variety of process parameters, considered with respect to welding of IS:2062 mild steel plate by means of gas metalarc welding process with a

copper coated mild steel wire of 0.8 mm diameter. A series of experiments was carried out to gather the data by means of Box-Behnken design method of RSM. Depending on the recorded data, the appropriate designs were introduced. Moreover, an effort was made to reduce the bead height and bead width and increase the DOP by means of the RSM technique.

In 2014, Jahanzaib, Wasim and Hussain (2014) introduced an average Ra representation of high strength low-alloy steel by exploiting multilayer coated carbide tools. Moreover, analysis was conducted, based on RSM, to establish the association among Ra and machining constraints. The feed rate was noted as the chief factor in determining surface roughness. Moreover, manipulation of feed versus speed and DOP showed that target Ra value can be attained via optimal combination of cutting factors. The accuracy of the introduced model has been established with confirmation data, yielding average calculation error of 3.38%.

In 2018, Vidyarthy and Dwivedi (2018) suggested a method, in which the effects of activating flux on weld bead geometry, heat input, and angular distortion of a single pass ATIG welding were assessed and compared with those for the traditional TIG welding. In addition, the ATIG welds, produced by means of MoO3 and CeO2 based activating flux, were examined under various measures. Moreover, it was noticed that the HI rises in the presence of activating fluxes with respect to the welding speed, welding current and arc length. Finally, the tensile strength of the proposed method was found to have improved when compared with BM.

Chandrasekar, Kailasanathan and Verma (2017) examined Inconel 600 plates by exploiting the ATIG welding process. In accordance with the results obtained, welding constraints were optimized, and appropriate flux was chosen prior to the joining of Inconel 600 plates, to generate the entire weld penetration in a single pass welding. Moreover, a variety of metallurgical and mechanical analyses were carried out on the UP-ATIG weldment. Finally, the investigations demonstrated that the tensile failure may happen in the weld zone and the tensile strength of weld joint was much lower when compared with the BM, owing to tensile residual stresses and coarser grain structures in the weld zone.

Gao et al. (2016) suggested a model, in which GA and the kriging scheme (KM) were applied for optimizing the process parameters. A four-factor, five-level study using Taguchi L25 design was carried out for various measures. In addition, KM was employed to estimate the association among various process parameters. The KM, which was developed, was exploited for parameter optimization by GA in order to increase DP, reduce BW and ascertain that the value of BR remains at a required level. Moreover, the influence of process parameter values on weld geometry was examined. Finally, the confirming experiments demonstrate that the attained optimum values were in excellent agreement with the results of the investigation.

Finally, Ragavendran et al. (2017) considered the hybrid laser TIG welding steel factors that were analyzed by combining a TIG welding heat source with a pulsed laser beam. The dataset was generated on the basis of the weld bead

measurement performed. Multiple regression designs, associating the process parameters with the responses were developed. The accuracy of the identified model was found to be improved over those obtained from other schemes. Subsequently, the desirability approach was exploited for determining the optimum process parameters (OPP) to attain the required weld bead profile. Finally, the experiments were performed based on the determined OPP, and improved results were obtained.

2.2. Assessment

Table 1 sums up the previously mentioned methods, features, and challenges of the conventional techniques regarding the optimizations of TIG welding parameters. Thus, RSM was suggested by Korra, Vasudevan and Balasubramanian (2014), as offering high accuracy with the rapid search for the optimum process settings. However, when current is low, BW is also reduced. Then, RSM was also proposed in Vasantharaja and Vasudevan (2015), assuring better torch speed and tip angle along with improved RMSE values. Anyhow, variations in welding current could still cause important changes in the DOP values. Afterwards, Box Behnken design was applied by Srivastava and Garg (2017), preferred as a better tool for the related optimization. The error is minimized in this scheme, but the increased travel speed leads to incomplete fusion. It should be noted that RSM was also suggested by Jahanzaib, Wasim and Hussain (2014) for reasons of providing better prediction accuracy and process. However, this becomes insignificant due to high speed and depth of penetration. A-TIG weldments were suuested by Vidyarthy and Dwivedi (2018), with the purpose of minimizing the toughness of weld zone with improved tensile strength and hardness, but there were occurrences of lower hardness profile. Further, laser shock penning (LSP) was implemented by Chandrasekar, Kailasanathan and Verma (2017) to improve efficiency and the signal to noise ratio. Its effects, though, showed residual compressive stresses. In turn, KM and GA were proposed by Gao et al. (2016), with which optimization is more uniform and with increased accuracy. This study, though, did not devote sufficient consideration to error analysis. Finally, the desirability approach was presented in Ragavendran et al. (2017), offering low distortion with reduced RMSE values. A drawback of this scheme is, however, constituted by the lower quality weld shape and non-uniform micro-structure. The limitations and challenges mentioned have to be considered in terms of improving the optimizations of TIG welding parameters in the current research work.

3. Design of the experiment

3.1. Objectives

For attaining the desired research objectives, the analysis here reported has been performed according to the following sequence of goals:

Table 2. Review of the state-of-the-art in the choice of TIG welding parameters

Reference	*Methodology*	*Features*	*Challenges*
Korra, Vasudevan and Balasubramanian (2014)	RSM	- High accuracy. - Offers rapid search for optimum process.	When current is low, BW is also reduced
Vasantharaja and Vasudevan (2015)	RSM	- Better torch speed and tip angle. - Offers improved RMSE values	The variation in welding current exerts great impact on DOP values
Srivastava and Garg (2017)	Box Behnken Design	- Better tool for optimization. - Error is minimized.	Increased travel speed leads to incomplete fusion
Jahanzaib, Wasim and Hussain (2014)	RSM	- Better prediction accuracy. - Increased productivity.	Insignificant due to high speed and depth of penetration
Vidyarthy and Dwivedi (2018)	SEM	- Minimizes the toughness of weld zone. - Improved tensile strength and hardness.	Occurrence of lower hardness profile
Chandrasekar, Kailasanathan and Verma (2017)	LSP	- Increased efficiency. - Better signal to noise ratio.	Occurrence of compressive residual stresses
Gao et al. (2016)	Kriging model and GA	- Increased accuracy. - Optimization is more uniform.	No much consideration on error analysis
Ragavendran et al. (2017)	Desirability approach	- Low distortion. - Reduced RMSE values.	More complicated structure

- To identify the significant metal inert gas welding constraints, which bear an important effect on weld bead geometry.
- To identify the lower and upper limits of the considered factors.
- To establish the design matrix relative to the investigation.
- To carry out a group of experiments based on the modeled matrix.
- To record the responses.
- To introduce the mathematical models.
- To verify the adequacy of the model obtained.

3.2. Materials under study

The structural material used in the analysis is 15CDV6 Steel (HSLA steel). This material is used in pressure vessels, rocket motor casings, etc. The list of welding process parameters exploited in the preparation of the welding process is given in Table 4.

3.3. Parameters and their values

The initial process parameters, affecting the weld bead geometry, expressed through DOP, BW and HAZ width, have been selected via literature exploration and numerous lab analyses. The selected five parameters are: W_c, T_s, G_r, T_a and A_g, and five levels were given for each of these input parameters.

3.4. Experimental procedure

The intention of this analysis is to optimize GTAW parameter values by means of RSM, in order to establish the maximum DOP, minimum BW and minimum HAZ width for autogenous welding with bead on plate trials. The design of the respective experiment is realised by means of RSM, based on CCD and then the sampling was carried out using Design Expert software. The entire setting of experiments is meant for finding the optimal parameter combinations.

The design matrix was constructed and analyzed for the 6.2 mm thick rolled plates of 15CDV6 steel to determine the possible working limits of the current GTAW parameter values. Various combinations of process parameter values were tried out in order to find the variable working limits of every process parameter. The bead appearance, bead contour, as well as weld quality were scrutinized to recognize these working limits of the parameters used for welding, leading to the observations listed below:

- If W_c is below 160 A, incomplete penetration or inadequacy of fusion occurs. On the other hand, if W_c is above 200 A, excessive melting or burn through could be noticed, owing to increased input of heat.
- If T_s is below 60 mm/min, more burn and swelling could be noticed. For T_s above 100 mm/min, inadequacy of very shallow penetration and fusion could be observed.
- If G_r is below 8 ltr/min, porosities are noticed in the weld bead owing to inadequate shielding. On the other hand, if G_r is above 16 ltr/min,

Table 3. Materials included in the welding process

Materials/ Constraints	*Description*	*Properties*
Bead on plate	Dimensions: 100 mm × 100 mm × 6.2 mm	• Unique interface in parts and assembly • No performance lag in the model • Auto-creation of welding symbol • Works with gaps or any practical geometry which can be welded. • Very efficient in creation especially with smart weld selection tool
Electrode	2% thoriated tungsten electrode of 3.2 mm diameter	• High tensile strength, ductility, corrosion resistance
Polarity	DCEN	• Straight polarity results in faster melt-off of the electrode and therefore faster deposition rate
SG	Pure argon	• Low thermal conductivity and ionization potential

production of porosities was noticed, owing to agitated flow gas and more utilization of the shielding gas (SG) would cause an increase in the welding cost.

- If T_a is below 70^0 and above 110^0, the SG flows far from the weld metal, and hence porosities can be noticed in the bead. The bead is noted to be wider in one direction and in addition to that, shallow penetration was also found out.
- If A_g is below 1.5 mm, electrode may be found to be stuck to the workpiece. On the other hand, if A_g is above 3.5 mm, initiation of the arc will be complicated, and the possibility of spatter occurrence will appear.

3.5. The design matrix

By taking into account the entire set of the above conditions, the possible ranges of the variables are selected such that the 15CDV6 plate should have been welded devoid of any defects. Owing to a variety of variables, it is decided to check 5 levels of 5 parameters, rotatable central composite, and to use the design matrix in order to determine the optimum values of the parameters considered.

The process parameters used and their selected values are specified in Table 3. Based on the design matrix, thirty-two sets of parameter settings and relative responses are provided in Table 5. In this table, first sixteen rows correspond to the half factorial (2^{5-1} =16) model and the subsequent ten rows show the axial or star points. The last six rows indicate the points at the centre. The distance of the axial runs from the centre is given by α. The selection of α is essential for the computation of the model. For sustaining the rotation capacity, α must be based on the number of simulations in the factorial portion of the central composite design, as shown in Eq. (1):

$$\alpha = [\textit{Number of factorial runs}]^{1/4} \tag{1}$$

If the factorial is in fact the half factorial, Eq. (2) can be formulated, in which k denotes the count of factors.

$$2 = [2^{k-1}]^{\frac{1}{4}} \text{ meaning, of course, that here } k = 5 \tag{2}$$

Table 4. Process parameters and their working ranges

Parameter	Notation	Units	Coded values				
			-2	-1	0	+1	+2
Welding current	W_c	Ampere	160	170	180	190	200
Torch speed	T_s	mm/min	60	70	80	90	100
Gas flow rate	G_r	ltr/min	8	10	12	14	16
Torch angle	T_a	degree	70	80	90	100	110
Arc gap	A_g	mm	1.5	2	2.5	3	3.5

All of the parameters are coded as (0), when their values are determined by the centre points. Moreover, in the mixture of all the constraints their upper or lower values are coded as (+2) and (-2). The mixture of every parameter with the remaining 4 parameter values at their of middle levels determines the star points. Therefore, the thirty-two experimental settings permitted the evaluation of linear, quadratic and two-way interactive influence of the process parameters on the responses of the GTAW. The range of every variable has been limited to a lower value (-2) and upper value (+2). The coded values are given by Eq. (3) and, moreover, the actual and coded values could be related by means of Eq. (4), where X_2 denotes the needed code value of a parameter X, X being any value of this parameter between the limits X_{min} and X_{max}, X_{min} denoting the lower limit and X_{max} the upper limit of the values considered:

$$Coded\,value = \frac{Actual\,value - Means}{Half\,of\,range} \tag{3}$$

$$X_2 = \frac{[2X - (X_{\max} + X_{\min})]}{X_{\max} - X_{\min}}. \tag{4}$$

3.6. Conducting the experiments and recording the responses

According to the proposed procedure of analysis, 15CDV6 plate of 6.2 mm thickness is exploited as base material. For determining the chemical composition of a BM, the AES technique was exectuted on various elements, and the results are presented in Table 5. Before the proper welding process, the plate is dimensioned to 100 mm ×100 mm ×6.2 mm by means of EDM and buffing subsequent to cleaning with acetone to eradicate the sample surface impurities (Montgomery, 1991). Kemppi master TIG MLS 4000 welding machine was used in this study along with automatic torch travel setup as shown in Fig. 1. The image of bead on plate trail and the image of the milled specimen are shown in Fig. 2 and Fig. 7, respectively.

A single pass autogenous TIG welding along with Direct Current Electrode Negative (DCEN) power source are applied for forming the bead on plate trails. A high purity argon (employed as shielding gas) and the 2% thoriated tungsten electrode with the diameter of 3.2 mm were used in the experiments. The sample is sliced in transverse direction by means of a power hacksaw machine, which is similar to the milling process. The samples are further grounded and polished and etched to assess the macrostructure in a precise manner. The etching process is finished by using a unique etchant, namely glycergia. The appearance of macrostructure and weld are viewed by means of an optical microscope. The DOP, BW and HAZ width are evaluated with the assistance of image J software. Moreover, the macrograph of thirty-two beads on plate trails is shown in Fig. 8.

The actual values of the parameters, evaluated voltage and relative HI are presented in Table 7. The HI is evaluated by means of Eq. (5), in which W_c

Table 5. Design matrix with experimental responses (W_c given in Ampere, T_s in mm/min, G_r in ltr/min, T_a is a degree and A_g is given in mm)

Design matrix							Responses		
SI No:		Coded values					DOP (mm)	BW (mm)	HAZ width (mm)
Std	Run	W_c	T_s	G_r	T_a	A_g			
15	1	-1	1	1	1	-1	2.495	8.5	2.192
6	2	1	-1	1	-1	1	3.012	11.375	3.481
11	3	-1	1	-1	1	1	2.827	10.792	2.183
4	4	1	1	-1	-1	1	2.653	10.708	2.696
8	5	1	1	1	-1	-1	2.403	9.267	2.635
12	6	1	1	-1	1	-1	3.812	9.482	2.302
1	7	-1	-1	-1	-1	1	2.665	10.917	3.392
14	8	1	-1	1	1	-1	3.057	11.829	2.491
5	9	-1	-1	1	-1	-1	2.747	9.473	3.043
9	10	-1	-1	-1	1	-1	3.607	9.462	3.478
3	11	-1	1	-1	-1	-1	2.139	8.667	2.748
2	12	1	-1	-1	-1	-1	3.116	13.167	3.082
7	13	-1	1	1	-1	1	2.118	9.499	2.213
13	14	-1	-1	1	1	1	2.606	10.833	2.696
10	15	1	-1	-1	1	1	3.469	10.917	3.579
16	16	1	1	1	1	1	2.635	11.058	3.016
17	17	-2	0	0	0	0	1.911	7.878	2.193
18	18	2	0	0	0	0	2.959	11.483	2.725
19	19	0	-2	0	0	0	3.398	12.625	4.144
20	20	0	2	0	0	0	2.795	10.708	2.599
21	21	0	0	-2	0	0	2.823	11.631	2.843
22	22	0	0	2	0	0	1.952	10.638	2.409
23	23	0	0	0	-2	0	2.415	9.917	2.353
24	24	0	0	0	2	0	3.397	10.542	2.597
25	25	0	0	0	0	-2	3.114	8.749	2.542
26	26	0	0	0	0	2	2.699	11.75	2.712
32	27	0	0	0	0	0	2.448	10.601	2.197
31	28	0	0	0	0	0	2.324	11.208	2.297
28	29	0	0	0	0	0	2.365	10.583	2.167
29	30	0	0	0	0	0	2.739	10.998	2.333
30	31	0	0	0	0	0	2.531	10.333	2.438
27	32	0	0	0	0	0	2.752	10.458	2.157

indicates the welding current, V denotes voltage, W_s signifies welding speed and η corresponds to efficiency:

$$HI = \eta \times \frac{W_c \times V \times 60}{W_s \times 1000} KJ/mm \tag{5}$$

For both pulsed and constant current gas, TIG process, the arc efficiency is found to be 70%.

Table 6. Chemical composition of the base material (% by weight)

Base material	15CDV6 steel
C	0.152
Cr	1.229
Mn	0.838
Mo	0.791
Ni	0.234
V	0.198
Si	0.189
Cu	0.107
P	0.005
Al	<0.02
S	<0.01
Fe	Balance

4. Modeling TIG welding: regression analysis

4.1. Regression analysis for DOP

The final regression equation of the model derived with respect to actual factors after neglecting the insignificant terms is specified subsequently.

$$\begin{aligned} DOP = {} & 13.20158 + 0.021037W_c - 0.332467T_s + 0.636135G_r \\ & -0.082811T_a - 0.616151A_g + 0.000786T_s * T_a \\ & -0.008216G_r * T_a - 0.018463T_a * A_g + 0.001521T_s^2 + \\ & 0.001045T_a^2 + 0.418538A_g^2 \end{aligned} \tag{6}$$

The ANOVA description and model summary statistics, obtained in terms of DOP analysis are provided in Tables 8 and 9, respectively. In addition, the contour plots which were examined on the basis of DOP, are shown in Fig. 3.

4.2. Regression analysis for BW

The final regression equation of the model for BW is given by Eq. (7).

$$\begin{aligned} BW = {} & -90.38908 + 1.23006W_c - 0.603165T_s + 7.64967A_g \\ & -0.070325\,W_c * A_g + 0.075375\,T_s * A_g - 0.000472\,G_r \\ & *T_a - 0.002733\,W_c^2 + 0.002232T_s^2 \end{aligned} \tag{7}$$

Table 7. Arc voltage and heat input of bead on plate trials

Run	Variable values					Arc voltage (volt)	Heat input (KJ/mm)
	W_c Ampere)	T_s (mm/min)	G_r (ltr/min)	T_a (degree)	A_g (mm)		
1	170	90	14	100	2	14.7	1.166
2	190	70	14	80	3	15.9	1.813
3	170	90	10	100	3	16.4	1.301
4	190	90	10	80	3	16.1	1.428
5	190	90	14	80	2	14.8	1.312
6	190	90	10	100	2	16.3	1.445
7	170	70	10	80	3	14.8	1.510
8	190	70	14	100	2	16.1	1.835
9	170	70	14	80	2	15.4	1.571
10	170	70	10	100	2	15.2	1.550
11	170	90	10	80	2	15.5	1.230
12	190	70	10	80	2	16.2	1.847
13	170	90	14	80	3	15.5	1.230
14	170	70	14	100	3	15.1	1.540
15	190	70	10	100	3	16.5	1.881
16	190	90	14	100	3	16.4	1.454
17	160	80	12	90	2.5	14.3	1.201
18	200	80	12	90	2.5	16.4	1.722
19	180	60	12	90	2.5	15.6	1.966
20	180	100	12	90	2.5	16.7	1.263
21	180	80	8	90	2.5	16.0	1.512
22	180	80	16	90	2.5	16.1	1.521
23	180	80	12	70	2.5	15.8	1.493
24	180	80	12	110	2.5	16.9	1.597
25	180	80	12	90	1.5	15.0	1.418
26	180	80	12	90	3.5	17.9	1.692
27	180	80	12	90	2.5	16.8	1.588
28	180	80	12	90	2.5	16.4	1.550
29	180	80	12	90	2.5	16.3	1.540
30	180	80	12	90	2.5	16.3	1.540
31	180	80	12	90	2.5	16.5	1.559
32	180	80	12	90	2.5	16.8	1.588

Table 8. ANOVA table for the depth of penetration analysis

Source	Sum of squares	df	Mean square	F-value	p-value	Validation	Contribution percentage
Model	6.41	20	0.3207	15.77	<0.0001	Significant	
A-W_c	1.06	1	1.06	52.24	<0.0001	Significant	16.31
B-T_s	1.02	1	1.02	50.36	<0.0001	Significant	15.70
C-G_r	0.2055	1	0.2055	10.11	0.0088	Significant	3.16
D-T_a	1.32	1	1.32	64.7	<0.0001	Significant	20.32
E-A_g	0.8078	1	0.8078	39.73	<0.0001	Significant	12.43
AB	0.0501	1	0.0501	2.46	0.1449	Not significant	
AC	0.0281	1	0.0281	1.38	0.2642	Not significant	
AD	0.0004	1	0.0004	0.0182	0.895	Not significant	
AE	0.0015	1	0.0015	0.072	0.7935	Not significant	
BC	0.0074	1	0.0074	0.3659	0.5575	Not significant	
BD	0.0988	1	0.0988	4.86	0.0497	Significant	1.52
BE	0.0016	1	0.0016	0.0777	0.7856	Not significant	
CD	0.432	1	0.432	21.25	0.0008	Significant	6.65
CE	0.0332	1	0.0332	1.63	0.2275	Not significant	
DE	0.1363	1	0.1363	6.71	0.0252	Significant	2.10
A^2	0.0082	1	0.0082	0.4037	0.5382	Not significant	
B^2	0.6482	1	0.6482	31.88	0.0001	Significant	9.98
C^2	0.024	1	0.024	1.18	0.3005	Not significant	
D^2	0.2994	1	0.2994	14.72	0.0028	Significant	4.61
E^2	0.3001	1	0.3001	14.76	0.0027	Significant	4.62
Residual	0.2237	11	0.0203				
Lack of Fit	0.0544	6	0.0091	0.2677	0.9302	Not significant	
Pure Error	0.1693	5	0.0339				2.61
Cor Total	6.64	31					100.00

Figure 1. Image of Kemppi master TIG MLS 4000 welding machine with automatic torch travel setup

Table 9. Model summary statistics for the depth of penetration analysis

Statistics	Values	Statistics	Values
Std. Dev.	0.1426	R^2	0.9663
Mean	2.75	Adjusted R^2	0.9050
C.V. %	5.19	Predicted R^2	0.7472
Press	1.68	Adeq Precision	16.180

The ANOVA description and model summary statistics related to BW analysis are provided in Tables 10 and 11, respectively. Moreover, the contour plots that were analyzed regarding the BW are specified in Fig. 4.

4.3. Regression analysis for HAZ

The final regression equation of the model, formulated with respect to the HAZ width is given by Eq. (8).

$$\begin{aligned} HAZ = {} & +72.55671\text{-}0.216452W_c\text{-}0.683835T_s\text{-}1.95003G_r \\ & \text{-}8.81772A_g{+}0.000806W_c * T_s{+}0.005066W_c * G_r{+} \\ & 0.040487W_c * A_g{+}0.006084T_s * G_r{+}0.002694T_s^2{+} \\ & 0.020755G_r^2{+}0.333077A_g^2 \end{aligned} \tag{8}$$

The ANOVA description and model summary statistics, determined in the framework of HAZ analysis are provided in Tables 12 and 13, correspondingly.

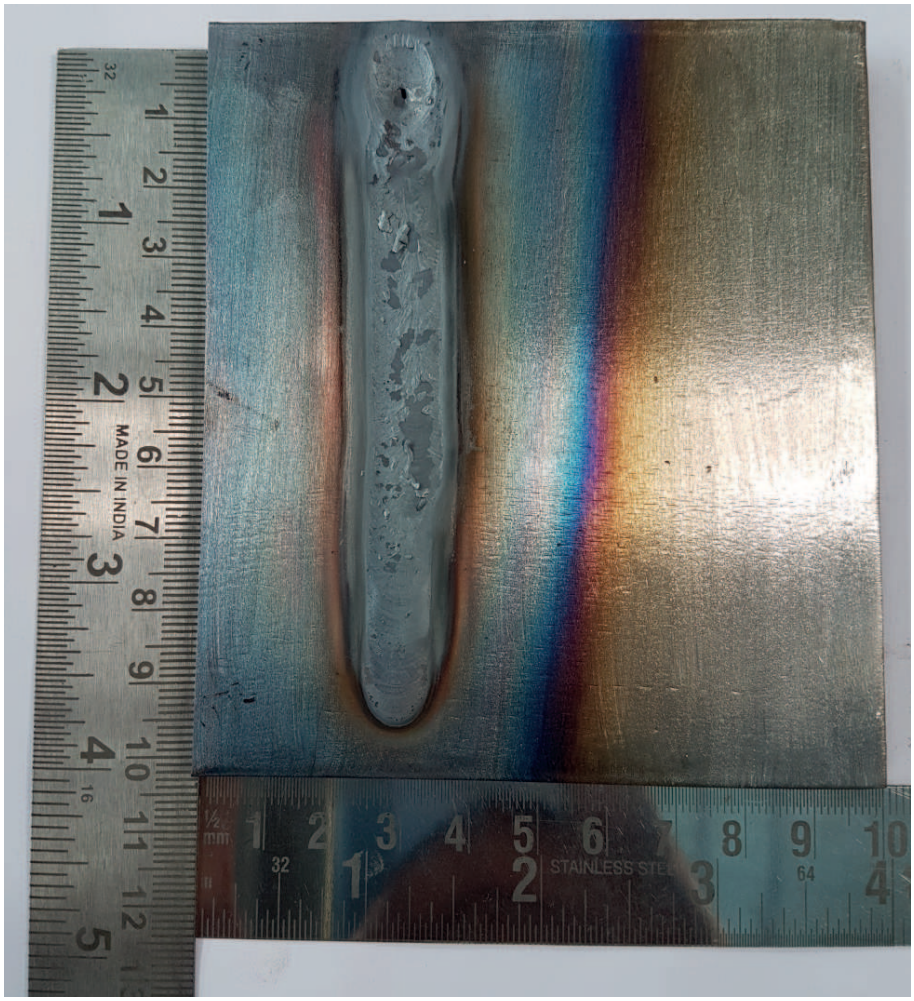

Figure 2. Image of autogenous GTAW welding of 15CDV6 plate

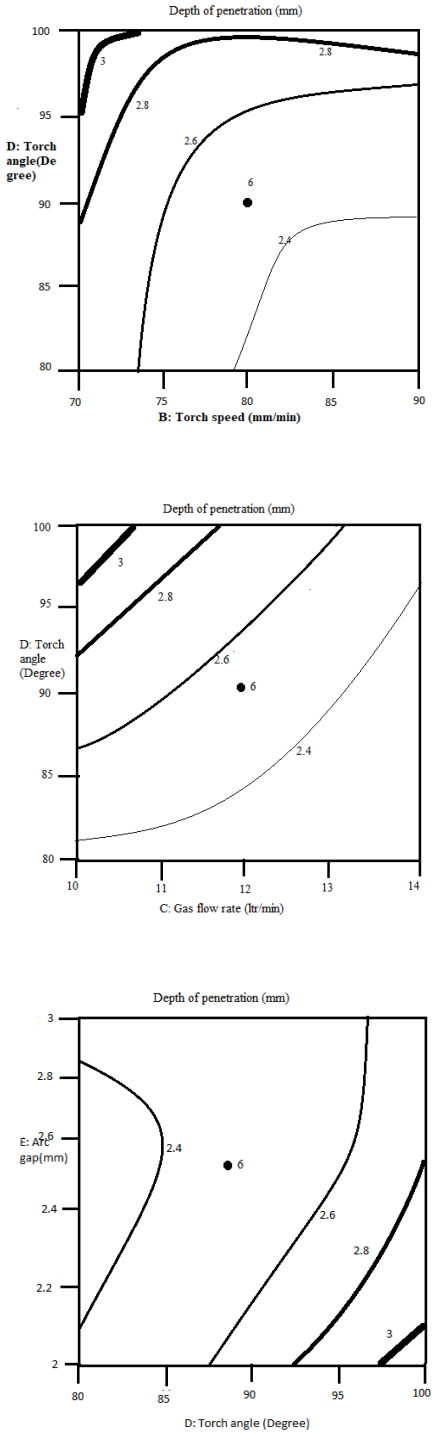

Figure 3. Countour plots for DOP analysis for (a) T_a vs. T_s; (b) T_a vs. G_r; (c) A_g vs. T_a

Table 10. ANOVA table for BW analysis

Source	Sum of squares	df	Mean square	F-value	p-value	Validation	Contribution percentage
Model	40.84	20	2.04	10.14	0.0002	Significant	
A-W_c	11.86	1	11.86	58.9	<0.0001	Significant	32.53
B-T_s	7.97	1	7.97	39.61	<0.0001	Significant	21.86
C-G_r	0.7576	1	0.7576	3.76	0.0785	Not significant	
D-T_a	0.0459	1	0.0459	0.2282	0.6422	Not significant	
E-A_g	6.26	1	6.26	31.08	0.0002	Significant	17.17
AB	0.7859	1	0.7859	3.9	0.0738	Not significant	
AC	0.0388	1	0.0388	0.1928	0.6691	Not significant	
AD	0.3198	1	0.3198	1.59	0.2336	Not significant	
AE	1.98	1	1.98	9.83	0.0095	Significant	5.43
BC	0.0086	1	0.0086	0.043	0.8396	Not significant	
BD	0.8019	1	0.8019	3.98	0.0713	Not significant	
BE	2.27	1	2.27	11.29	0.0064	Significant	6.23
CD	1.83	1	1.83	9.09	0.0118	Significant	5.02
CE	0.0812	1	0.0812	0.4035	0.5383	Not significant	
DE	0.3606	1	0.3606	1.79	0.2078	Not significant	
A^2	2.46	1	2.46	12.2	0.005	Significant	6.75
B^2	1.26	1	1.26	6.25	0.0295	Significant	3.46
C^2	0.161	1	0.161	0.7998	0.3903	Not significant	
D^2	0.6791	1	0.6791	3.37	0.0934	Not significant	
E^2	0.6352	1	0.6352	3.16	0.1033	Not significant	
Residual	2.21	11	0.2013				
Lack of fit	1.65	6	0.2752	2.44	0.173	Not significant	
Pure error	0.5636	5	0.1127				1.55
Cor Total	43.06	31					100.00

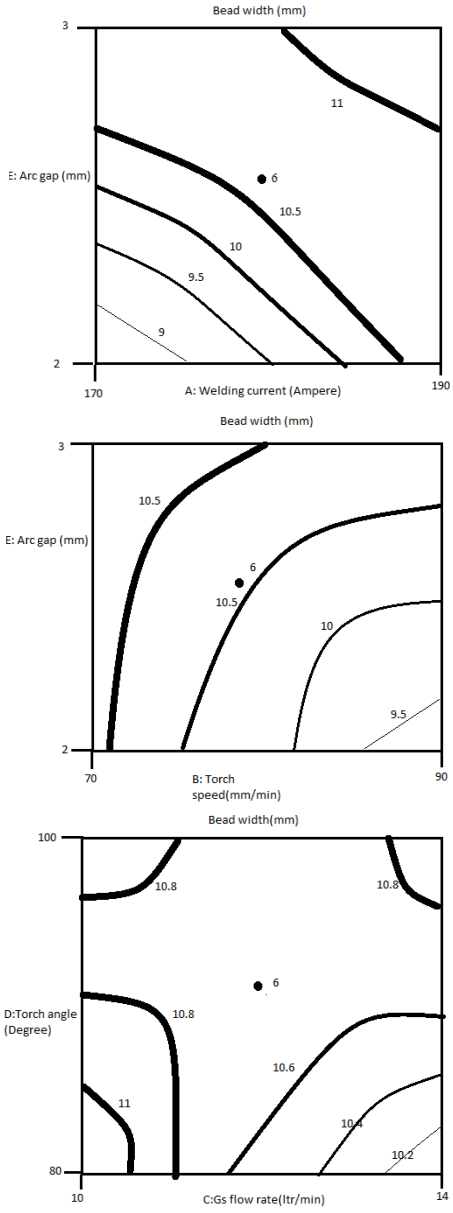

Figure 4. Countour plots for BW: (a) A_g vs. W_c; (b) A_g vs. T_s; (c) T_a vs. G_r

Table 11. Model summary statistics for BW analysis

Statistics	Values	Statistics	Values
Std. Dev.	0.4487	R^2	0.9486
Mean	10.5	Adjusted R^2	0.8551
C.V. %	4.27	Predicted R^2	0.6918
Press	44.43	Adeq. precision	13.6489

Then, the contour plots, related to the analysis of HAZ, are presented in Fig. 5.

5. Optimization of welding parameters

5.1. The Response Surface Methodology

In the framework of the design of experiments, the RSM technique (Montgomery, Myers and Anderson, 2009) takes a very prominent position. It is a compilation of numerical and statistical methods constructive for the modeling and examination of issues arising in a situation, where the response of interest depends upon numerous variables, and the intention is to optimize this response (Cornu, 1998; Dupont and Marder, 1995).

For instance, the development of a plant is influenced by a particular quantity of water, x_1, and sunshine, x_2. The plant can grow in conditions of any treatment (x_1,x_2). In fact, in real conditions, sunshine and water supply can vary incessantly. When treatments are offered from a continuous range of values, the RSM assists in determining the improved or optimized conditions with respect to the response variable. Accordingly, the plant growth, Y is the response variable for this illustrative example and it depends upon the operation of sunshine and water. This dependence can take the form as in Eq. (9):

$$Y = F(x_1, x_2) + \in . \tag{9}$$

The variables x_1 and x_2 are independent variables on which the response Y depends. The dependent variable Y is a function of x_1 and x_2 and the error term, denoted $\in$. The error term encompasses all kinds of measurement errors involved in the variables here appearing, as well as the very response function, F. It is represented by a variable, supposed to be distributed normally with variance S^2 and zero mean.

In the majority of RSM applications, the F is unknown. With the intention of developing an appropriate estimation for F, the experimenter generally commences with a low-order polynomial, valid in a certain small region. This approximating function is a first order representation, if the response can be described by a linear function of independent variables. A first-order representation with two independent variables can be as given in Eq. (10). A higher degree polynomial could be exploited, if there exists a curvature in the response

Table 12. ANOVA table for HAZ analysis

Source	Sum of squares	df	Mean square	F-value	p-value	Validation	Contribution percentage
Model	7.39	20	0.3697	19.09	<0.0001	Significant	
A-W_c	0.2733	1	0.2733	14.12	0.0032	Significant	3.65
B-T_s	2.9	1	2.9	149.94	<0.0001	Significant	38.76
C-G_r	0.11	1	0.11	5.68	0.0363	Significant	1.47
D-T_a	0.0312	1	0.0312	1.61	0.2306	Not significant	
E-A_g	0.2402	1	0.2402	12.41	0.0048	Significant	3.21
AB	0.1038	1	0.1038	5.36	0.0409	Significant	1.39
AC	0.1642	1	0.1642	8.48	0.0141	Significant	2.19
AD	0.0073	1	0.0073	0.3754	0.5525	Not significant	
AE	0.6557	1	0.6557	33.87	0.0001	Significant	8.76
BC	0.2369	1	0.2369	12.24	0.005	Significant	3.17
BD	0.0015	1	0.0015	0.0776	0.7858	Not significant	
BE	0.0423	1	0.0423	2.19	0.1673	Not significant	
CD	0.0226	1	0.0226	1.17	0.3033	Not significant	
CE	0.0405	1	0.0405	2.09	0.176	Not significant	
DE	0.0339	1	0.0339	1.75	0.2123	Not significant	
A^2	0.0708	1	0.0708	3.66	0.0822	Not significant	
B^2	2.25	1	2.25	116.47	<0.0001	Significant	30.07
C^2	0.2423	1	0.2423	12.52	0.0047	Significant	3.24
D^2	0.0828	1	0.0828	4.28	0.063	Not significant	
E^2	0.2436	1	0.2436	12.58	0.0046	Significant	3.26
Residual	0.213	11	0.0194				
Lack of fit	0.1515	6	0.0252	2.05	0.2234	Not significant	
Pure error	0.0615	5	0.0123				0.82
Cor. total	7.61	31					100.00

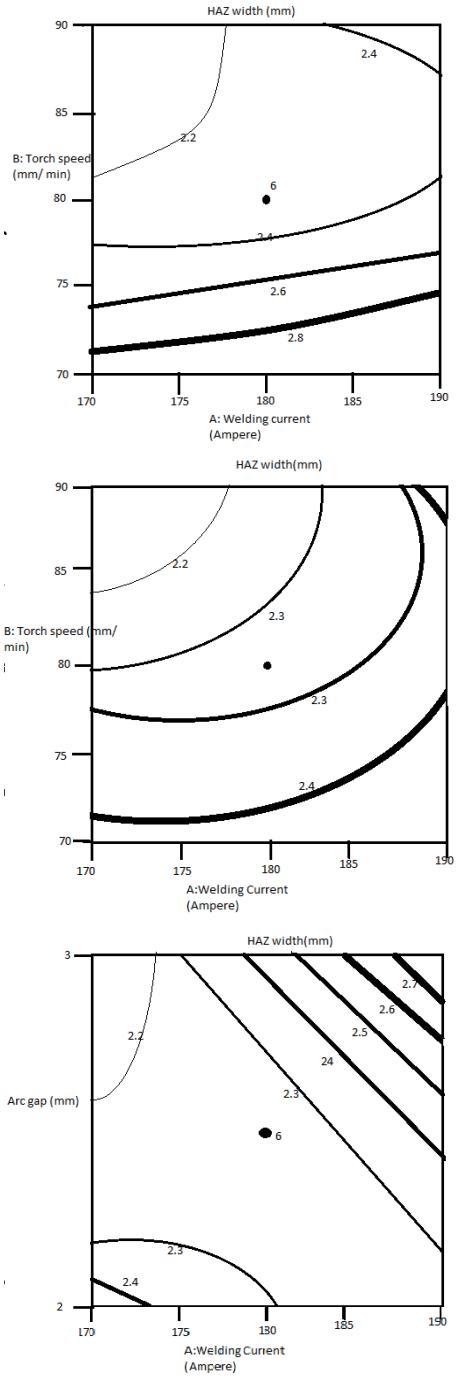

Figure 5. Countour plots for HAZ: (a) T_s vs. W_c; (b) G_r vs. W_c; (c) A_g vs. W_c

Table 13. Model summary statistics for HAZ analysis

Statistics	Values	Statistics	Values
Std. Dev.	0.1391	R^2	0.9720
Mean	2.69	Adjusted R^2	0.9211
C.V. %	5.18	Predicted R^2	0.7544
Press	4.15	Adeq Precision	17.3395

surface. A function with two variables is said to be a second-order model when given by a simile of Eq. (11):

$$Y = a_0 + a_1x_1 + a_2x_2 + \in \tag{10}$$

$$Y = a_0 + a_1x_1 + a_2x_2 + a_{11}x_{112} + a_{22}x_{222} + a_{12}x_1x_2 + \in . \tag{11}$$

Generally, the RSM technique usually refers to either one or the combination of both of these representations. In each design, the values of the factors considered are independent of the values of various other parameters. For attaining the most proficient outcome in the approximation of polynomials, the appropriate model has to be applied with the purpose of collecting information. Once the information is collected, the technique of least squares is employed to assess the coefficients in the polynomials. The response surface investigation is carried out by employing the fitted surface. Hence, the objective of analyzing RSM can be achieved by the subsequent steps:

- Comprehending the topography of the response surface.
- Identifying the region, in which the optimal response appears. The objective is to shift speedily and effectively along a path to obtain a minimum or a maximum response so that the response is optimized.

5.2. Optimized results

In the proposed framework, Design Expert 11 software was used to perform the optimization via the RSM approach. The optimization criteria for RSM or the process parameters and response constraints are given in Table 14, and the desired solutions that depend on the criteria are provided in Table 15.

6. Validation

The optimized parameter values were verified by conducting five confirmatory tests. For confirmatory tests, a new set of process parameter values was taken into account. The experiment was carried out, and the bead profile geometry for the selected optimal solution was evaluated. The differences between the experimental and predicted values and the root mean square errors were measured and are shown in Table 16. Also, it was noted that the RMSE (root means

Table 14. Process parameters and response constraints or optimisation criteria for RSM

Name	Goal	Lower limit	Upper limit	Lower weight	Upper weight	Importance
A: W_c	within range	160	200	1	1	3
B: T_s	within range	60	100	1	1	3
C: G_r	within range	8	16	1	1	3
D: T_a	within range	70	110	1	1	3
E: A_g	within range	1.5	3.5	1	1	3
DOP	target = 4.5	1.911	4.5	1	1	5
BW	target = 8	8	13.167	1	1	3
HAZ width	target = 2.5	2.5	4.144	1	1	3

square error) is below 2%, i.e. within the tolerable range (Luo et al., 2018). Hence, the optimized parameter values were shown to offer improved results, i.e. the maximum DOP and minimum BW and HAZ width.

7. Practical implications

TIG welding is a process that is used to join thin metals. It produces a joint that matches the original metals in chemical composition, making the bond highly resistant to corrosion and cracking over the long term. The adequate precision of TIG welding is highly desirable in the manufacture of, for instance, medical devices. TIG welding offers a solution for welding critical joints in medical devices; and for situations, in which small or exceptionally precise welds are required. It produces a high-quality and high-purity weld compared with other joining processes, which is crucial in many applications. The price of TIG welding services is also usually quite affordable. Overall, it is most efficient way to manufacture medical devices, as well as for other purposes here mentioned. That is why improvement in this kind of process is of importance.

8. Conclusions

This paper has presented a way to improve the welding technique, known as TIG welding, using RSM algorithm for enhancing the TIG welding process

Table 15. Obtained solutions depending on criteria

Number	W_c	T_s	G_r	T_a	A_g	DOP	BW	HAZ width	Desirability
1*	184.212	93.125	10.311	106.16	1.56	4.5	8	2.5	1
2	182.653	90.967	9.116	102.419	1.5	4.5	8	2.5	1
3	175.836	86.589	9.098	110	1.984	4.5	8	2.5	1
4	182.193	93.9	8.847	102.911	1.653	4.5	8	2.5	1
5	171.869	93.75	8.151	110	2.457	4.5	8	2.5	1
6	174.724	89.385	8.3	109.959	2.268	4.5	8	2.5	1
7	181.827	91.22	8.441	104.713	1.825	4.5	8	2.5	0.997
8	175.54	84.399	10.267	110	1.675	4.5	8	2.5	0.995
9	175.85	84.87	11.154	110	1.5	4.5	8	2.5	0.993
10	182.835	96.128	8.898	102.675	1.709	4.5	8	2.5	0.99
11	178.774	97.477	9.285	105.903	1.926	4.5	8	2.5	0.989
12	173.891	95.202	8.005	108.047	2.339	4.5	8	2.5	0.989
13	177.365	97.809	11.503	110	1.775	4.5	8	2.5	0.987
14	173.119	92.505	8	110	2.515	4.5	8	2.5	0.986
15	174.904	83.094	10.671	109.999	1.568	4.5	8	2.5	0.983
16	166.817	94.289	8.061	110	2.686	4.5	8	2.5	0.981
17	176.756	83.668	9.294	110	1.914	4.5	8	2.5	0.98
18	176.899	90.654	8.174	109.93	2.432	4.5	8	2.5	0.98
19	183.33	91.72	8	105.496	2.071	4.5	8	2.5	0.978
20	192.042	98.951	8.86	97.14	1.501	4.5	8	2.5	0.975

*Selected

Table 16. Validation test results

No.	W_c	T_s	G_r	T_a	A_g		DOP	BW	HAZ width
1	184.212	93.125	10.311	106.16	1.56	Experimental	4.188	9.336	2.848
						Predicted	4.5	8	2.5
2	171.869	93.75	8.151	110	2.457	Experimental	3.784	8.728	2.048
						Predicted	4.5	8	2.5
3	175.85	84.87	11.154	110	1.5	Experimental	3.897	9.086	2.214
						Predicted	4.5	8	2.5
4	166.817	94.289	8.061	110	2.686	Experimental	3.478	8.469	2.013
						Predicted	4.5	8	2.5
5	192.042	98.951	8.86	97.14	1.501	Experimental	3.886	9.507	3.298
						Predicted	4.5	8	2.5
						RMSE value	0.6921	1.0941	0.5062

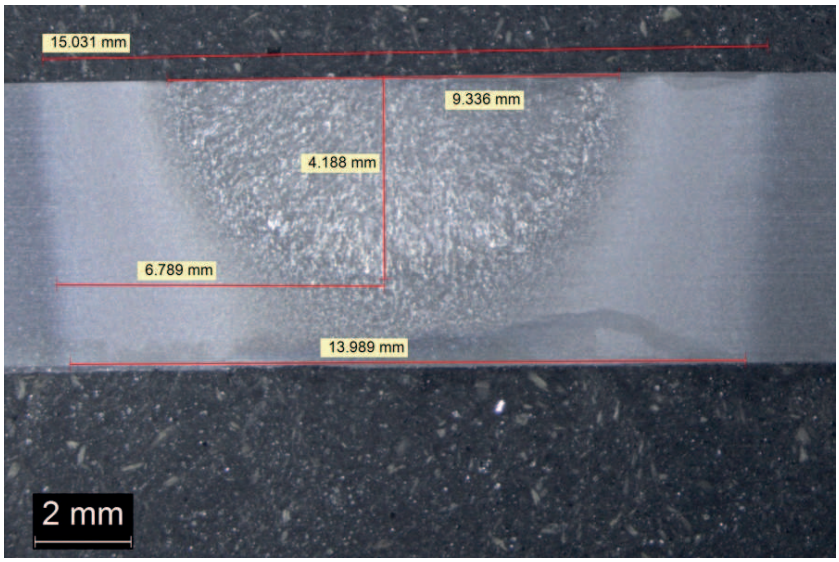

Figure 6. Macrostructure of the selected optimal solution

parameters regarding the weld bead profile of 15CDV6 HSLA steel. Moreover, it turned out to be possible to identify the conditions of optimal welding by means of multi-objective optimization of RSM with respect to increase of the DOP value and decrease of BW and HAZ width. The variables, accounted for in the model considered were W_c, T_s, G_r, T_a and A_g. The simulations were performed showing different values of DOP, BW and HAZ widths. Moreover, the contour plots, surface plots, and process parameters were analyzed for the responses considered. The implemented scheme was also analysed with regards to normal plot, predicted vs. actual plot, residual vs. predicted plot, and residual vs. run plot, and the expected outcomes were achieved. Finally, the outcomes obtained from the implemented model were found to be extremely beneficial to rocket-motor hardware program, for industries and fabrication of pressure vessels, and other branches that use the 15CDV6 steel.

References

Ai, Y., Shao, X., Jiang, P., Li, P., Liu, W. (2016) Welded joints integrity analysis and optimization for fiber laser welding of dissimilar materials. *Optics and Lasers in Engineering*, 86, 62-74.

Chandrasekar, G., Kailasanathan, C., Verma, D.K. (2017) Investigation on un-peened and laser shock peened weldment of Inconel 600 fabricated by ATIG welding process. *Materials Science and Engineering: A*, 690, 405-417.

Figure 7. Photograph of milled specimens

Chellappan, M., Lingadurai, K., Sathiya, P. (2017) Characterization and Optimization of TIG welded supermartensitic stainless steel using TOPSIS. *Materials Today: Proceedings*, **4**(2): 1662-1669.

Chen, J., Wu, C.S., Chen, M.A. (2014) Improvement of welding heat source models for TIG-MIG hybrid welding process. *Journal of Manufacturing Processes*, **16**(4): 485-493.

Chen, J., Zong, R., Wu, C., Padhy, G.K., Hu, Q. (2017) Influence of low current auxiliary TIG arc on high speed TIG-MIG hybrid welding. *Journal of Materials Processing Technology*, 243, 131-142.

Chen, Q., Lin, S., Yang, C., Fan, C., Ge, H. (2017) Grain fragmentation in ultrasonic-assisted TIG weld of pure aluminum. *Ultrasonics Sonochemistry*, 39, 403-413.

Chinchole, P.N.K.P. (2016) Medical Image Fusion using YCbCr Colour Transformation. *International Journal of Computer Science Trends and Technology*, **4**(4).

Cornu, J. (1998) *Advanced welding system, TIG and related process, Part 2.* IFS Publication Ltd., UK, 97–123.

Costa, J.D., Sousa, M.B., Fook, N.C.M.L., Alves, J.J.N., Santana, R.A.C. (2016) Obtaining and characterization of Ni-Ti/Ti-Mo joints welded by TIG process. *Vacuum*, 133, 58-69.

DuPont, J.N. and Marder, A.R. (1995) Thermal efficiency of arc welding processes. *Welding Journal*, **74**(12).

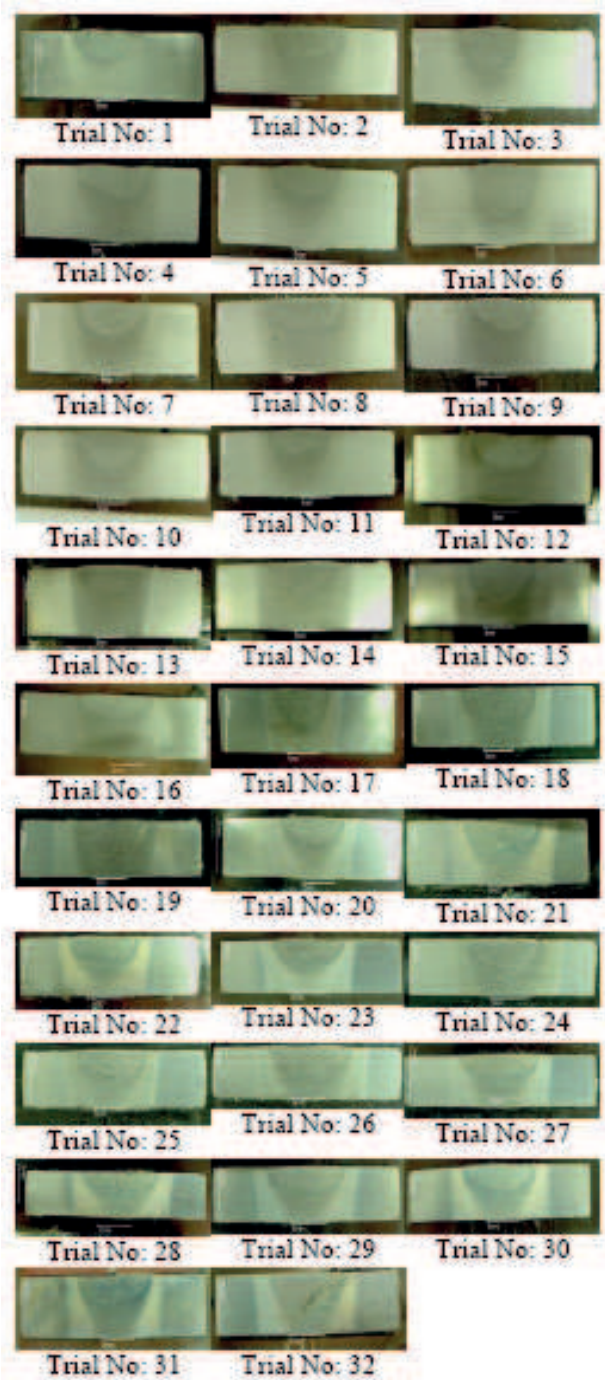

Figure 8. Macrograph of autogenousTIG welded bead on plate trials

Gao, Z., Shao, X., Jiang, P., Cao, L., Wang, C. (2016) Parameters optimization of hybrid fiber laser-arc butt welding on 316L stainless steel using Kriging model and GA. *Optics & Laser Technology*, 8, 153-1623.

Hirose, T., Sakasegawa, H., Nakajima, M., Tanigawa, H. (2015) Mechanical properties of TIG and EB weld joints of F82H. *Fusion Engineering and Design*, 98–99, 1982-1985.

Jahanzaib, M., Wasim, A., Hussain, S. (2014) Surface roughness modeling using RSM for HSLA steel by coated carbide tools. *International Journal of Advanced Manufacturing Technology* **78**(5-8), 1031–1041.

Junaid, M., Baig, M.N., Shamir, M., Khan, F.N., Haider, J. (2017) A comparative study of pulsed laser and pulsed TIG welding of Ti-5Al-2.5Sn titanium alloy sheet. *Journal of Materials Processing Technology*, 242, 24-38.

Korra, N.N., Vasudevan, M., Balasubramanian, K.R. (2014) Multi-objective optimization of activated tungsten inert gas welding of duplex stainless steel using response surface methodology. *The International Journal of Advenced Manufacturing Technology*, **77**(1-4), 67–81.

Liang, Y., Hu, S., Shen, J., Zhang, H., Wang, P. (2017) Geometrical and microstructural characteristics of the TIG-CMT hybrid welding in 6061 aluminum alloy cladding. *Journal of Materials Processing Technology*, 239, 18-30.

Longlong, G., Hualin, Z., Shaohu, L., Yueqin, L., Chunyu, F. (2016) Formation Quality Optimization and Corrosion Performance of Inconel 625 Weld Overlay Using Hot Wire Pulsed TIG. *Rare Metal Materials and Engineering*, **45**(9): 2219-2226.

Luo, X., Chen, X., Wang, T., Pan, S., Wang, Z. (2018) Effect of morphologies of martensite–austenite constituents on impact toughness in intercritically reheated coarse-grained heat-affected zone of HSLA steel. *Materials Science and Engineering: A*, 710, 192-199.

Meng, X., Qin, G., Zhang, Y., Fu, B., Zou, Z. (2014) High speed TIG–MAG hybrid arc welding of mild steel plate. *Journal of Materials Processing Technology*, **214**(1): 2417-24241.

Montgomery, D.C. (1991) *Design and Analysis of Experiments, 3.* John Wiley, New York.

Montgomery, D.C., Myers, R.H., Anderson C,M. (2009) *Response Surface Methodology, 3.* John Wiley, New York.

Nagesh, D.S., Datta, G.L. (2010) Genetic algorithm for optimization of welding variables for height to width ratio and application of ANN for prediction of bead geometry for TIG welding process. *Applied Soft Computing*, **10**(3): 897-907.

Nelson, T.W. and Rose, S.A.(2016) Controlling hard zone formation in friction stir processed HSLA steel. *Journal of Materials Processing Technology*, 231, 66-74.

Piekarska, W., Rek, K. (2017) Numerical Analysis and Experimental Research on Deformation of Flat Made of TIG Welded 0H18N9 Steel. *Pro-*

cedia Engineering, 177, 182-187.

Prasad, V.M.V., Varghese, V.M.J., Suresh, M.R., Kumar, D.S. (2016) 3D Simulation of Residual Stress Developed During TIG Welding of Stainless Steel Pipes. *Procedia Technology*, 24, 364-371.

Ragavendran, M., Chandrasekhar, N., Ravikumar, R., Saxena, R., Bhaduri, A.K. (2017) Optimization of hybrid laser – TIG welding of 316LN steel using response surface methodology (RSM). *Optics and Lasers in Engineering*, 94, 27-36.

Shi, Y., Zheng, Z., Huang, J. (2013) Sensitivity model for prediction of bead geometry in underwater wet flux cored arc welding. *Transactions of Nonferrous Metals Society of China*, **23**(7): 1977-1984.

Singh, A.K., Dey, V., Rai, R.N. (2017) Techniques to improve weld penetration in TIG welding (A review). *Materials Today: Proceedings*, **4**(2): 1252-1259.

Srirangan, A.K., Paulraj, S. (2016) Multi-response optimization of process parameters for TIG welding of Incoloy 800HT by Taguchi grey relational analysis. *Engineering Science and Technology, an International Journal*, **19**(2): 811-817.

Srivastava, S., Garg, R.K. (2017) Process parameter optimization of gas metal arc welding on IS:2062 mild steel using response surface methodology. *Journal of Manufacturing Processes*, 25, 296-305.

Thompson, S.W. (2018) Fine–scale structural features of intercritically aged HSLA-100 plate steel and their influence on yield strength and low-temperature impact toughness. *Materials Characterization*, 136, 425-434.

Vasantharaja, P. and Vasudevan, M. (2015) Optimization of A-TIG welding process parameters for RAFM steel using response surface methodolog. *J. Materials: Design and Applications*, 1-16.

Vidyarthy, R.S., Dwivedi, D.K. (2018) Microstructural and mechanical properties assessment of the P91 A-TIG weld joints. *Journal of Manufacturing Processes*, 31, 523-535.

Wang, H., Yuan, X., Li, T., Wu, K., Xu, C. (2018) TIG welding-brazing of Ti6Al4V and Al5052 in overlap configuration with assistance of zinc foil. *Journal of Materials Processing Technology*, 251, 26-36.

Yan, G., Tan, M.J., Crivoi, A., Li, F., Chia, C.H.N. (2017) Improving the mechanical properties of TIG welding Ti-6Al-4V by post weld heat treatment. *Procedia Engineering*, 207, 633-638.

Yang, X., Deng, W., Zou, L., Zhao, H., Liu, J. (2013) Fatigue behaviors prediction method of welded joints based on soft computing methods. *Materials Science and Engineering: A*, 559, 574-582.

Zou, J.L., Wu, S.K., Xiao, R.S., Li, F. (2015) Effects of a paraxial TIG arc on high-power fiber laser welding. *Materials & Design*, 86, 321-327.